Chapter 1

Introduction

Using current technology has become a standard feature of daily life in the modern world. These technologies have many useful uses that improve functionality and standard of life. Among them, one of the terms utilized in modern technology the most often is magnetism. Simple devices like compasses and electrical generators give way to computers and other advanced technology; cassettes and videotapes give way to pen drives and hard drives; magnetism transforms the world.

1.1 Magnetism: An Introduction

Magnetic materials attract or repel one another through a force called magnetism, essentially the result of the movement of electrical charges, or electrical current. Every material is built up of microscopic particles referred to as atoms, and these atoms are made up of nuclei, which are the centers of mass around which electrons spin. The magnetization of a material is entirely determined by the electronic configuration of its component ions. In most materials, equal numbers of electrons spin in opposing directions, canceling out their magnetization and resulting in zero magnetic moments; however, if any unpaired electron exists, the system will have a net magnetic moment. As a result, magnetic substances can therefore be classified as diamagnetism, paramagnetic, ferromagnetism, antiferromagnetism, and ferrimagnetism.

1.1.1 Diamagnetism

The ability of an ion or material to counteract an applied magnetic field is known as diamagnetism. Lenz's law describes the diamagnetic behavior of a substance. Lenz's law states that any change in the magnetic flux passing through a current loop surrounding a magnetic field will result in a current in the loop that opposes the change in flux. As a result, changes in any external field lead all atoms to exhibit some degree of diamagnetism. This

occurs as a result of electron orbital motion around a nucleus. However, every material has an innate diamagnetism caused by quantum mechanical phenomena. The substance diamagnetic shows paired electrons. Thus, the outcome is zero net magnetization. The susceptibility of these materials is negative.

1.1.2 Paramagnetism

Paramagnetic materials have at least one unpaired electron. They exhibit a low but positive magnetic susceptibility. The permanent magnetization of paramagnetic materials is caused by the spins of the unpaired electrons in their atoms, molecules, and ions. Without external magnetic fields, these moments are arbitrarily directed since atom spins do not interact or only very weakly interact with the spins of surrounding atoms, resulting in zero net magnetization. Whenever an external magnetic field is applied to such materials, the spins align in the direction of the applied magnetic field, resulting in a net attraction in the direction of the magnetic field. As soon as the external magnetic field disappears, they will demagnetize. The magnetic field will tend to arrange the spin moment of every atom, whereas the thermal energy of the temperature will randomize the spin moment which is shown in Fig 1.1.

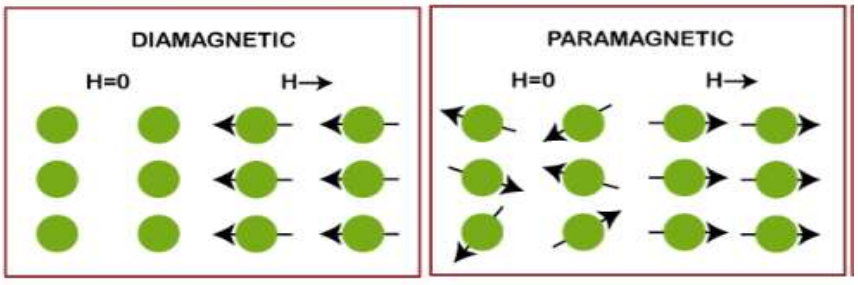

Figure 1.1: *Schematic presentation of spin alignment in microscopic structures of diamagnetic and paramagnetic materials both in the absence and in the presence of a magnetic field H.*

1.1.3 Ferromagnetism

Even though ferromagnetic materials have unpaired electrons, their magnetic susceptibilities are extremely high and positive, and they can maintain their magnetism even after the applied extrinsic magnetic field has disappeared. In ferromagnetic materials, spin alignment is parallel to that of their surrounding spins. These spins aligned with the direction of the magnetic field when an extrinsic magnetic field was applied. The development of a magnetic domain provides an understanding of the ferromagnetism process.

1.1.4 Antiferromagnetism and ferrimagnetisms

Spin alignment in antiferromagnetic substances is antiparallel to the surrounding spin alignment shown in Fig 1.2. As a result, they have a zero net magnetic moment. Magnetization is canceled by reciprocal cancellation. Similarly, the ferrimagnetic material possesses two anti-aligned magnetic sub-lattices, but the magnetic moments are of different strengths. Thus, a ferrimagnetic substance possesses a net magnetization.

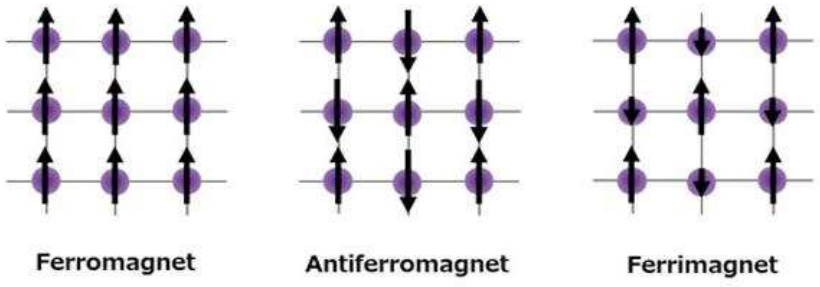

Figure 1.2: *Schematic representation of spin alignment in ferromagnetic, antiferromagnetic, and ferrimagnetic materials.*

1.2 Rules define the different types of magnetic ordering

1.2.1 Curie –Weiss Law

Curie-Weiss law illustrates the relationship between temperature (T), magnetic susceptibility (χ), Curie-Weiss temperature (θ), and Curie constant (C). This law is defined as

$$\frac{1}{\chi} = \frac{T}{C} - \frac{\Theta}{C} \tag{1}$$

The Curie-Weiss temperature (θ) can be used to clarify the many magnetic ordering types that a material has. The relationship between temperature and inverse magnetic susceptibility for various substances is depicted in Fig 1.3.

(i) For paramagnetic materials; $\theta = 0$ K

(ii) For ferromagnetic materials θ = positive value

(iii) For negative value for antiferromagnetic materials θ = negative value.

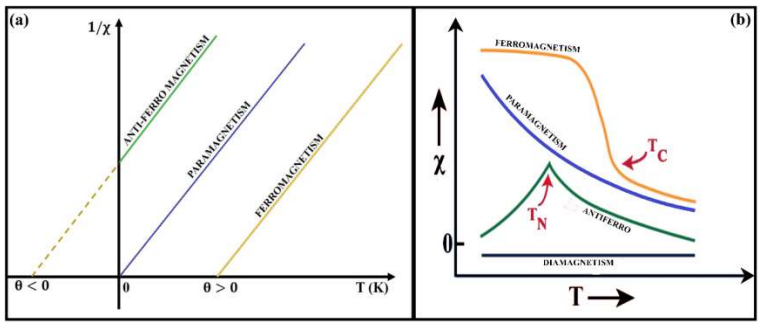

Figure 1.3: *Temperature variation of inverse magnetic susceptibility for paramagnetic, ferromagnetic and antiferromagnetic material.*

1.2.2 Landau's theory of ferromagnetism (mean field theory):

Free energy is expressed as:

$$F(M) = F_0 + a(T)M^2 + bM^4 \quad (2)$$

Where F_0 and b are the constants (b > 0) and $a\,(T)$ is the temperature-dependent parameter. The proper phase transition occurred when $a\,(T)$ becomes: $a\,(T) = a_0(T - Tc)$, where a_0 is known as the proper constant.

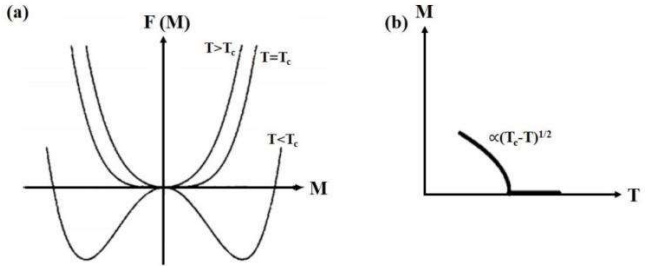

Figure 1.4: (a) Free energy *vs.* magnetization curve. (b) Magnetization *vs.* temperature graph.

For the minimization of the free energy:

$$\frac{\partial \mathrm{F}}{\partial \mathrm{M}} = 0 \quad (3)$$

$$2M\,[a_0(T - Tc) + 2bM^2]$$

$$M = 0 \; or \; M = \pm\,[\frac{\mathrm{a0(T-\,Tc)}}{2b}]^{1/2}$$

The first term is applicable for the above and below Tc while the second term is considered only below Tc. It provides an unstable equilibrium ($\partial^2\mathrm{F}/\partial^2 M$) for $T < Tc$. Thus, below Tc,

the magnetization is proportional to $(Tc - T)^{1/2}$ as shown in Fig.1.4 along with the variation of free energy with magnetization.

1.3 Perovskite Material

1.3.1 Single Perovskite Material:

In the Russian Ural Mountains, Gustav Rose made the initial discovery of perovskite material in 1839. The Russian Mineralogist L. A. Perovski is the name it is named for similar to calcium titanium oxide ($CaTiO_3$), perovskite material has the same crystal structure. ABX_3 is the formula of perovskite material, where the B-site ion sits in the center of the lattice and the A-site ion is usually an alkaline earth or rare earth element shown in Fig 1.5. B-site elements are often transitional 3d, 4d, or 5d elements. The figure demonstrates the structure of a cubic perovskite unit cell. The interaction between the electron, spin degrees of freedom, and lattice makes it difficult for the cubic or undistorted structure of a type of compound to survive. As a result, the symmetry decreases to a tetragonal, orthorhombic, or trigonal configuration.

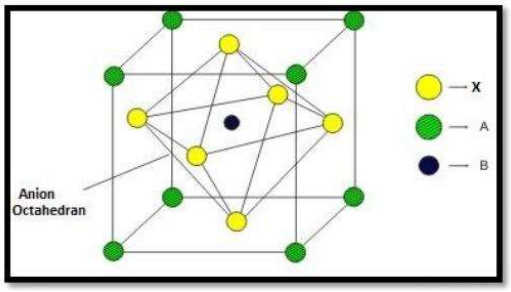

Figure 1.5: *Show the crystal structure of ABX_3 perovskite.*

1.3.2 Double Perovskite Material:

It is obvious from the term "Double Perovskite (DP)" that two perovskites must be used, specifically $ABX_3.AB'X_3$. As a result, $A_2BB'O_6$ is formed, which is the typical chemical

formula for DP. In the DP crystal structure, two unit cells of a single perovskite are alternately repeated [1]. The formation of DP from a single perovskite cell is displayed in Fig 1.6. The unit cell of the DP has six oxygen atoms coupled with B and B'-site (transition metal) ions [2]. The DP structure is formed by the 3-dimensional repetition of the octahedral BO_6 and $B'O_6$. Various magnetic phases such as FM, AFM, SG/CG, etc. can be found in these materials due to the varying possible combinations of B and B' ions. Furthermore, the valence states and ionic radius of B/B' ions determine the kind of magnetic ordering that exists in the system. According to the Goodenough-Kanamori Rules, FM material occurs if the B/B' ions have different ionic radius and valance states [3]. Additionally, materials undergo AFM according to the same criteria if B^{3+}/B'^{3+} have the same ionic states. The Goldschmidt tolerance factor (t) is used to calculate the geometrical stability of DPs as

$$t = \frac{\frac{(2-x)r_A+(x)r_{A\prime}}{2}+r_O}{\sqrt{2}\left(\frac{r_B+r_{B\prime}}{2}+r_O\right)} \quad (4)$$

Where r_A, r_B, r_B', and r_O are the Shannon ionic radii of the A, B, and B' sites and oxygen ions, respectively. Interaction between charge and spin makes these materials more useful and applicable in daily use. Due to their usefulness in both electronics and magnetism, the research fields for these materials are extensive.

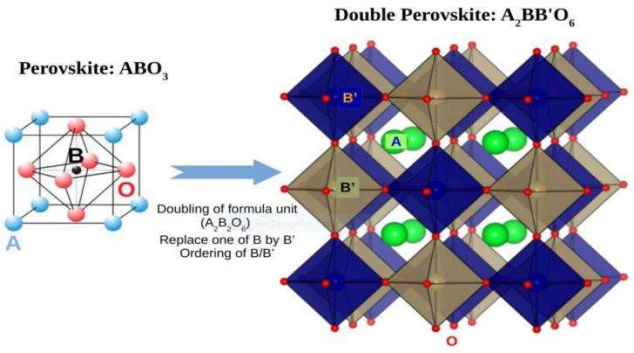

Figure .1.6: *Systematic diagram of the double perovskite material.*

1.4 Correlation between electronic structure and magnetism:

The magnetic nature of any system depends upon the different exchange interactions present in that system, and complex states, prior knowledge of the electronic structure and the spin state of elements present in the system is essential. It directly affects the magnetic features since different valence states have different magnetic moments and produce different exchange interactions. In particular, the electronic structure study for the oxides family having different transition metals has drawn great attention because of its ability to stabilize in different valence states as well as in different spin states i.e., different spin-state degrees of freedom. For example, in general, the Co/Mn/Fe/Ni transition metals can reside in 2+/3+/4+ oxidation states. Moreover, Co^{3+} ions, in octahedral coordination can exist in three possible spin states: a high spin (HS) state (S = 2, $t^4_{2g}eg^2$), a low spin (LS) state ($S = 0$, $t\ ^6_{2g}e^0g$), and even an intermediate spin (IS) state ($S = 1$, $t^5_{2g}e^1g$) which have the d^6 configuration. Similarly, the Co^{2+} ions which have the d^7 configuration in octahedral coordination can stay in the HS state (S = 3/2, $t^5_{2g}eg^2$) and LS state (S = 1/2,$t^6_{2g}e^1g$) [4–7]. Similarly, other transition metals also have various spin states such as Fe^{2+}, Ni^{2+}, Cr^{2+}, etc. Moreover, particularly related to our work, the ordered DP's are FM insulators showing high-temperature magnetic ordering transition via the 180^0 FM superexchange interactions between B^{2+} and B^{4+} ions (half-filled d orbital) and can be easily demonstrated by the Goodenough-Kanamori rule. For DP's, ASD's i.e., an exchange of B/B' sites are known to have well-known consequences for their properties, particularly their magnetic properties which call for rigorous experimental and theoretical explorations of their electronic structure. The ASD leads to significant deviations from ferromagnetism by producing additional AFM clustered regions. Moreover, the mixed valence state of transition metal also supports ASD

and creates AFM exchange interactions. All these AFMs can be understood via superexchange interactions in the form of B^{2+}-O^{2-}-B^{2+}, B^{3+}-O^{2-}-B^{2+}, B'^{4+}-O^{2-}-B'^{4+} and B'^{3+}-O^{2-}-B'^{3+} which further leads to the generation of competition between FM and AFM interaction [8–12]. In addition, the compounds having rare earth (4*f*) elements with magnetic properties exhibit a broad range of intriguing properties because of the competing 4*f*-3*d* exchange interactions additionally due to the localized and complex configuration of the 4*f* orbitals as compared to the transition metal (3*d*) orbitals. Thus, the study of the exact valence state is important to understand diverse interesting magnetic properties of the system and the magnetic anisotropy which leads to the competing complex interactions 3*d*-3*d*, 4*f*-4*f* consisting of anisotropic, isotropic symmetric, anti-symmetric, and 4*f*-3*d* superexchange [5,9,12]. The prior knowledge of the electronic structure also helps us to give a good estimation of the total magnetic moment of the system. For this purpose, X-ray photoemission spectroscopy (XPS) spectra and X-ray absorption (XAS) spectra are unique tools to probe into the oxidation state of the constitutive elements present in the system. Moreover, XAS can also probe into the spin states of the system.

1.5 A brief literature survey on R_2CoMnO_6 double perovskite

Recent research has focused a great deal of attention on different rare-earth-based double precipitation (DP) systems with B sites occupied by Co and Mn, or R_2CoMnO_6 (where R = La to Lu; rare earth elements). These systems have attracted interest because of a variety of intriguing functional properties, such as electrical and optical properties, defect-induced modulation of physical properties, tunable magnetization steps, magneto-caloric effect and pyro-current, magneto-resistance, exchange bias, magneto-caloric and magneto-dielectric

effects, clustered phase that is both Griffiths-like and non-Griffiths-like, spin-phonon coupling, Hopkinson effect, multiferroicity, etc. [13–24]. The R_2CoMnO_6 family exhibits large changes in the Co-O-Mn bond length and bond angle due to a modest change in rare-earth size. This leads to modifications in the magnetic and electronic ground states through super-exchange interactions. The corners of the lattice in these DP oxides are alternatingly occupied by the CoO_6 and MnO_6 octahedral. When the ionic radii of the rare-earth elements decline from La to Lu, the ordering temperature, T_C, linearly decreases from 204 K (for La_2CoMnO_6) to 48 K (for Lu_2CoMnO_6), resulting in a ferromagnetic ordering caused by dominating Co^{2+} and Mn^{4+}super exchange interactions [25]. However, due to the random distribution of Co/Mn ions, anti-ferromagnetic ordering also arises owing to Co^{2+}-O^{2-}- Co^{2+} and Mn^{4+}-O^{2-}-Mn^{4+} superexchange interaction along with dominant ferromagnetic phase [25,25,26,26,27]. Furthermore, at lower temperatures, the rare earth ions might produce more magnetic ordering, which would moderate the magnetic characteristics. For instance, in Er_2CoMnO_6, in contrast to the ferromagnetic ordering of the Co^{2+} and Mn^{4+} moments below 70 K, a ferromagnetic behavior has been seen below 30 K because of the long-range ordering of Er^{3+} moments with Co/Mn sublattice. Among the R_2CoMnO_6 family of double perovskites, the La_2CoMnO_6 has been the most investigated. It is a ferromagnetic insulator with a magnetic transition temperature of around 225 K when B-site atoms are perfectly ordered. However, due to partial anti-site disorder, La_2CoMnO_6 exhibits two successive ferromagnetic around 210 K (corresponding to Co^{2+}-O^{2-}-Mn^{4+} superexchange interaction) and 150 K (corresponding to Co^{3+}-O^{2-}-Mn^{3+} superexchange interaction) [28,29]. Another interesting aspect of the R_2CoMnO_6 family i.e., Lu_2CoMnO_6 also exhibits ferroelectricity, where magnetically ordered collinear Co-Mn-Co-Mn chains induce electrical polarization via

breaking of the spatial inversion symmetry and this coupling of the electrical and magnetic property was rather strong in its single crystal. In Lu_2CoMnO_6, a ↑↑↓↓ type spin ordering was observed beneath the ~ 43 K, while the ferroelectric ordering was observed below ~35 K. In this system, ↑↑↓↓ type magnetic ordering was also probed by neutron diffraction measurement [16,25,26].

1.6 Literature survey on A_2CoFeO_6 type Double Perovskite:

Extensive research and study on double perovskite (DP's) of the A_2CoMn/NiO_6 type have been reported. Therefore, we have focused on less explored DP in this thesis—that is, DP's of the A_2CoFeO_6 type. This is a brief overview of certain A_2CoFeO_6 type DP's that are being observed.

1.6.1 La_2CoFeO_6 System

In the double Perovskite family, the Lanthanum (La) ion is a commonly utilized A-site element. One of the most researched materials in the field is the La_2CoMn/NiO_6-based DP. La_2CoFeO_6 (LCFO) is categorized as an anti-ferromagnetic insulator. At T_N ~ 270 K, it demonstrates long-range anti-ferromagnetic ordering [30,31]. At lower temperatures, the structure of the system changes from a rhombohedra ($\bar{R}C$) structure at 300 K to an orthorhombic (Pnma) structure at 201 K. In the compound, this structural transition leads to significant irreversibility and thermal hysteresis. The neutron diffraction data demonstrates that the LCFO system has a G-type anti-ferromagnetic ordering. A magnetic moment of value 0.2 μ_B/f.u. was measured at 5 K, as determined by the isothermal magnetization curve of LCFO. Space group I_4/mmm was estimated by Monte Carlo computations [31].

1.6.2 Pr_2CoFeO_6 System

DP Pr_2CoFeO_6 (PCFO) is a fascinating material that exhibits nearly all of the magnetic features. Its electronic state analysis using the XAS and XPS instruments shows that the Fe and Co ions were in the same trivalent (+3) oxidation state. The PCFO sample is insulating since there are no electronic states present across the Fermi level. Furthermore, the AFM transition at $T_N \sim 269$ K is revealed by data on magnetization and neutron diffraction. For this material, a significant spin-phonon interaction has also been described. For PCFO, the B-site disordered orthorhombic (Pnma) structure has been used [32]. This system shows several extremely fascinating magnetic phases, including the exchange-bias effect, Griffith phase, long-range anti-ferromagnetic ordering, and reentrant cluster glass ($T_G \sim 34$ K) [33].

1.7 Some important physical phenomena related to our research

1.7.1 Griffiths phase

In an unusually strange magnetization known as the "Griffiths phase (GP)," regions or clusters that are magnetically correlated are formed inside the paramagnetic region just above the transition temperature. This regime is characterized by the formation of a short-range cluster, which causes the inverse DC magnetic susceptibility to deviate downward from the C-W plotted line (i.e., $\chi = C/(T - T_{CW})$) below a temperature called the Griffiths temperature (T_G). Therefore, to examine the existence of GP, one needs to measure the temperature variation of magnetization under different applied magnetic fields. The examined decrease in inverse susceptibility is most pronounced at smaller applied fields and diminishes at larger fields due to an increasing paramagnetic background. Inverse DC susceptibility in the GP region is determined by the power law, or modified C-W law [34–37], provided by

$$\chi^{-1}(T) = B\,[T - T_C^R/T_C^R]^{(1-\lambda)} \quad (5)$$

Where B is a constant and T_C^R is the critical temperature in the paramagnetic region, also referred to as the lowered temperature of the randomly distributed clustered. A defining exponent of GP λ varies between 0 and 1 for $T_C^R < T < T_{GP}$. The selection of the value of T_C^R has resulted in a value of λ that is nearly zero for $T > T_{GP}$ in the above equation. It follows that T_C^R will be near the Curie-Weiss temperature [38,39].

1.7.2 Meta-magnetism

Changes in temperature or magnetic fields can cause abrupt discontinuous jumps in magnetization, known as the "Meta-magnetic Transition (MMT)". The first-order magnetic transition between low- and high-magnetization states with low magnetic susceptibility in each state is responsible for the steps. The presence of anisotropy and many competing interactions typically leads to the MMT, which is caused by the spin's reorientation along the magnetic anisotropy direction. The most important feature of metamagnetism is the existence of meta-stable magnetic plateaus. This kind of discontinuity in magnetization can also result from spin flipping and lattice distortion induced by the magnetic field, which at certain point values of the applied magnetic field cause a transition from an AFM to an FM state. In this scenario, an increase in the magnetic field will attempt to induce FM domains to grow; nevertheless, the net magnetic moment will only slightly alter because of the strong pinning forces existing. There is a sudden rise in magnetization when the external field energy reaches a threshold value of the magnetic field and exceeds the energy associated with the FM/AFM APB (magneto-striction energy). There is a sudden rise in magnetization when the external field energy reaches a threshold value of the magnetic field and surpasses the energy

associated with the FM/AFM APB (magneto-striction energy). This happens when certain spins flop along the direction of the extrinsic field. The system reaches a new meta-stable state as a result of this process, which sees a decrease in magnetostatic energy and an increase in elastic energy. Increasing the extrinsic magnetic field further will cause the magnetic strength field to reach another crucial value, at which point it will again flop a few spins and initiate the second step in magnetization; thus, successive jumps from one metastable state to another precede overall transitions [40].

1.7.3 Exchange Bias Phenomenon

Exchange bias (EB) is a phenomenon in which a system's M-H loop shifts along the magnetic field axis. The Exchange-Bias effect is shown in the asymmetry of the M-H curve. The EB effect was initially identified in 1956 by Meiklejohn and Bean. They noticed that the antiferromagnetic oxide CoO had undergone a hysteresis shift. The EB effect can be obtained in a system where different inhomogeneous magnetic phases coexist. There are several possible combinations of magnetic phases that can coexist, including a soft/hard phase of FM, FM/AFM, FM/pin glass, FM/ferrimagnet, etc [41–44]. These days, EB-containing materials have several potential uses, including in spintronic, data storage, memory devices, and more. Both the EB field (H_{EB}) and the coercivity (H_C) of a system can be determined with these equations. In which the left and right coercive fields are denoted by H_L and H_R, $H_{EB} = (H_L + H_R)/2$ and $H_C = (|H_L| + |H_R|)/2$.

Explanation of exchange-bias effect:

The EB phenomenology seen in an FM/AFM structure is explained in Fig 1.6. The following five steps may assist you in understanding the process:

First: Exchange bias occurs in the FM/AFM material due to interface coupling at the boundary of FM/AFM layers when the material is cooled below the ordering temperature (T_C) of the ferromagnetic system but above the Neel temperature (T_N) of the antiferromagnetic system in the presence of a magnetic field ($T_N < T < T_C$). When an external field is applied, AFM spins are oriented arbitrarily in a paramagnetic state, while FM spins are aligned in the field direction.

Second: When $T < T_N$, an exchange interaction occurs between the AFM and FM spins in the first monolayer, coupling them along field direction across the interface. Another monolayer of AFM spins

Can follow the AFM nature i.e. associated anti-parallel to the previous one and it leads to a typical ferromagnetic hysteresis curve.

Third: Due to spin un-compensation at the FM/AFM associate, small finite magnetization is generated at the monolayer. FM and AFM both maintain a single-domain state during the magnetization reversal process. Due to the significant AFM anisotropy at the FM/AFM interface, only the FM spin begins to align in the magnetic field direction when the magnetic field is reversed, while the AFM spins remain in the same condition.

Fourth: When the extra reverse field is applied, all FM spins are aligned in that direction.

Furthermore, the FM/AFM boundary causes FM spins to become anti-parallel to AFM spins. Therefore, there is only one possible configuration for an FM spin.

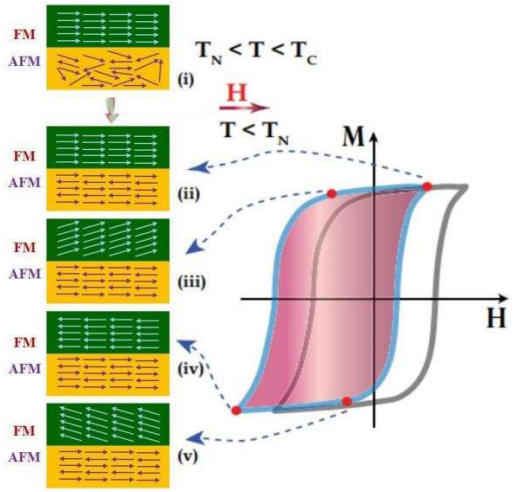

Figure 1.7: *systematic representation of exchange bias mechanism.*

Fifth: Since the FM spins are coupled with the AFM spins, they can easily flip when a positive field is applied, even at low magnetic fields. As such, the magnetic hysteresis loop moves away from its center and into the direction opposite to the magnetic field, a phenomenon known as exchange bias. Conventional exchange bias (CEB) refers to EB obtained in the presence of an extrinsic magnetic field. However, unexpectedly, EB can be observed even when no extrinsic magnetic field is present; therefore, the system still displays exchange bias even when no extrinsic magnetic field is present. This EB phenomenon is referred to as SEB or spontaneous exchanger bias. Recently, systems including SEB have become widely popular in the field of education [45,46].

1.7.4 Spin-glass

Spin glass (SG) is the new field of interest in magnetism where the spins behave differently from the conventional LRO instead of at low temperatures they behave collectively [47]. The term ‘glass’ is directly related to normal glass because the alignment of the spins looks random but does not change with time in these magnetic phases. The occurrence of the SG

phase has mainly these three reasons: competing interactions, randomness, and frustration. The disorderliness of glassy behavior occurs due to the following reasons such as site disorder which arises due to the randomization or disorderness of the distance among the magnetic moments, or due to randomization of the nearest neighbor interaction called bond randomness [48]. Moreover, in the system, the randomness in the strength of these interactions along with the mixed FM and AFM interactions causes frustration. Thus, the appearance of magnetic frustration caused by the competition between FM and AFM interactions results in the degenerate multiple magnetic ground states. In the experimental time scale, the equilibrium state is not achieved by the system during this procedure which is demonstrated by the memory effects, non-exponential decay, aging effects, slow spin-relaxations thermomagnetic irreversibility, etc. Thus, the disorder is the essential ingredient for inducing the glassy phase [49]. In contrast, when spin frustration or disorder is locally present in the area of the cluster known as a cluster glass (CG) phase [49].

1.7.5 Dielectric property

Dielectric materials are insulators that permit an electric field or flux to pass through them but not an electric charge when an electric field is applied externally. However, the electric charges are somewhat moved from their stable locations by the electric field, resulting in net dielectric polarization. From a technological perspective, various dielectric qualities are essential, including dielectric loss, dielectric strength, and relative permittivity (dielectric constant) of materials. The resistivity of a substance determines its static charges, while the permittivity of a material determines its electrical resistivity. The relative permittivity of the substances can be determined from the capacitance (C) measurement using the relation

$$K = C\ (d/k_0\ A) \quad (6)$$

Where d is the plate separation and A is the material's cross-sectional area. The dielectric constant can also be expressed in terms of real (ε') and imaginary (ε'') components, such that $\varepsilon* = \varepsilon' - i\varepsilon''$, as well as another physical variable called the loss tangent (dielectric loss), which is defined as $tan\ (\delta) = \varepsilon''/\ \varepsilon'$. A tangent loss is used to quantify the dissipation of dielectric, which can be related to several factors such as phonon interactions, crystal symmetry, the blockage between electrical signals and polarization, and many more.

1.8 Motivations of the thesis

Within the field of condensed matter research, disorder-driven spin frustration is one of the most exciting and promising subjects. These systems are highly interesting for further study because of their many features, including spin-phonon coupling, exchange bias, reentrant cluster glass state, high-temperature magnetic ordering, and single ion spin freezing.

Moreover, DPs having "A" site nonmagnetic ions such as La, Y, Lu, and Eu have recently drawn extensive attention due to their distinctive magnetic behavior. The most intriguing feature observed in Y_2CoMnO_6 and Lu_2CoMnO_6 is the meta-magnetic transition (MMT) in the isothermal magnetization curve [5,120–122]. Materials with the coexistence of MMT and giant magneto-caloric effect have great importance in solid-state cooling technology like highly efficient magnetically cooled refrigerators. The step positions change with temperature and sweep rate of the external magnetic field and also the steps are more prominent at a lower temperature. Eu_2CoMnO_6 with nonmagnetic Eu^{3+} is the much less studied system. The end members of this family are $EuMnO_3$ and $EuCoO_3$. In $EuMnO_3$, an incommensurate antiferromagnetic structure is observed at 52 K, and an *A*-type

antiferromagnetic ordering is found at 48 K. On the other hand, $EuCoO_3$ is a nonmagnetic compound even down to low temperature, the energy splitting in Co^{3+} ions between low spin (S=0) and the intermediate spin states (S=1) is ~2200 K. Starting from $EuMnO_3$, the ferrimagnetic spin ordering temperature increases with Co doping to 120 K and decreases for higher Co concentrations. Therefore, exploring the properties of Eu_2CoMnO_6 may unravel new interesting magnetic states. In this chapter, along with MMT, we have shown the existence of Griffiths-like phase, strong spin-glass-like behavior, and Hopkinson-like effect in Eu_2CoMnO_6.

The Co/Mn-based DP is extensively explored in the context of disorder-induced spin frustration. Co/Fe-based B-site disordered systems have received minimal attention. Furthermore, Co and Fe ions each have their characteristics, while having comparable size and valence states in the periodic table. The magnetic, and electrical, properties of La-based DP are fantastic. At the anti-ferromagnetic transition temperature (270 K), DP La_2CoFeO_6 exhibits a long-range ordering. However, in another DP the properties of Pr_2CoFeO_6 feature strong spin-phonon coupling, spin glass, exchange bias, and the Griffiths phase. Furthermore, a G-type of AFM ordering was found to occur below 269 K by neutron diffraction study. Therefore, we have changed the Pr ion in Pr_2CoFeO_6 DP to the La ion to see the lattice effect. The oxidation states of Co and Fe for this molecule are similar (+3). The $Pr_{1.8}La_{0.2}CoFeO_6$ compound's many characteristics have been studied. Different features in systems, such as large exchange bias and enormous magneto-resistance, have been traced back to hole doping in magnetic systems, as has been previously described. Furthermore, hole doping produces mixed valance states of B/B' ions.

The Y_2CoMnO_6 is another well-studied member of the R_2CoMnO_6 double perovskite family. It was much attracted owing to their meta-magnetism and ferroelectricity driven by the magneto-striction effect due to the E-type magnetic ordering of the Co^{2+}-Mn^{4+}-Co^{2+}-Mn^{4+} spin chain. However, the sharp steps in isothermal magnetization (meta-magnetic transition) have been credited to the anti-phase boundary among the magnetic moments emerging owing to the presence of anti-site disorder in the system. Later, it has also been supposed that the multiferroicity in the Y_2CoMnO_6 originated owing to defect dipoles, trapped charges, or any other extrinsic effects rather than the E-type magnetic ordering Other than this, Y_2CoMnO_6 also manifests multi-caloric effects simultaneously such as magneto-caloric and electro-caloric effects around its ferroic ordering temperature (~75 K). The Y_2CoMnO_6 has meta-magnetic properties. We doped Ca at the Y site to study the magnetic and electrical properties change. Ca (2+) changed oxidation state at the Y (3+) site and Ca has a larger ionic radius than Y. So it affects magnetic properties by arising ASD and lattice deformation of YCMO.

Chapter 2

Experimental Section

In Chapter II, many methods for material characterization and examination are thoroughly described, as is the process of producing the various samples used for our research work.

2.1 Sample preparation

Preparation of the sample is always the first step in experimental physics and material study. The experimental characterization and examination of the inherent physical properties of the sample, which can be easily compared with the various known theoretical models, require samples of acceptable quality (pure phase). In the present study, a solid-state reaction technique was used to synthesize several double perovskite compositions. Subsequently, the structural, magnetic, and transport characteristics of all the produced samples were measured.

2.1.1 Solid state reaction route

The most popular technique for preparing samples for oxide polycrystalline solids is the standard solid-state reaction method. To produce the desired product, the stoichiometric ratio of pure oxide powders was taken and ground in an agate mortar for an hour. This mixed material was first heated (calcination) in an air-filled muffle furnace for several days at a temperature lower than 1000–1100 ℃ to facilitate the reaction and the nucleation of the occurring phase. After cooling, the mixture was reground and subjected to increasing temperatures (1150–1250 ℃) for several days while being ground intermittently to promote more reaction and the formation of product nuclei (this process is called sintering). In such a scenario, the sintered powder was converted into pellets using a hydraulic press at a pressure after the XRD analysis demonstrated the presence of a pure phase. The pellets were then placed at a high temperature (1350–1400 ℃) for a few days to complete the sintering

process. These pellets were used to investigate their various properties, such as electrical, structural, magnetic, spectroscopic, optical, and so on.

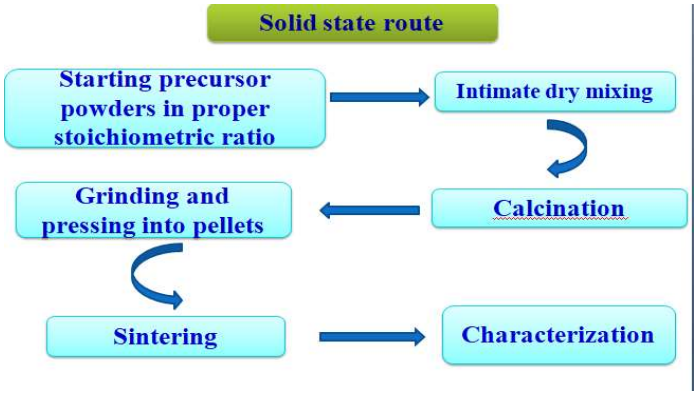

Figure 2.1: *Procedure of sample preparation using the solid-state route.*

2.2 Experimental characterization techniques

This section discusses the significance and function of the many characterization approaches that we utilized during our research.

2.2.1 X-ray diffraction measurement

The “X-ray diffraction (XRD)" technique is one of the most significant techniques for qualitatively and quantitatively analyzing the phase and crystal structure of any crystalline or polycrystalline material. The configuration of atoms, ions, and molecules on their crystallographic sites is correlated with many physical properties of materials, especially electrical, magnetic, and optical properties. Thus, the measurement of the X-ray diffraction spectrum becomes important since structural information is revealed to be essential to the research of materials.

Fundamental Principle: Sir William H. and Sir W. Lawrence Bragg's discovery of Bragg's Law serves as the foundation for X-ray diffraction. Bragg's Law specifies the

relationship between the angles at which a specific wavelength X-ray beam diffracts from a crystalline lattice.

Mathematically $2d \sin\theta = n\lambda$ (7)

Where, d = Inter plane distance of atoms, n = Integer displaying the diffraction peak order. λ= wavelength of X-rays, θ= Scattering angle or Bragg‘s Law.

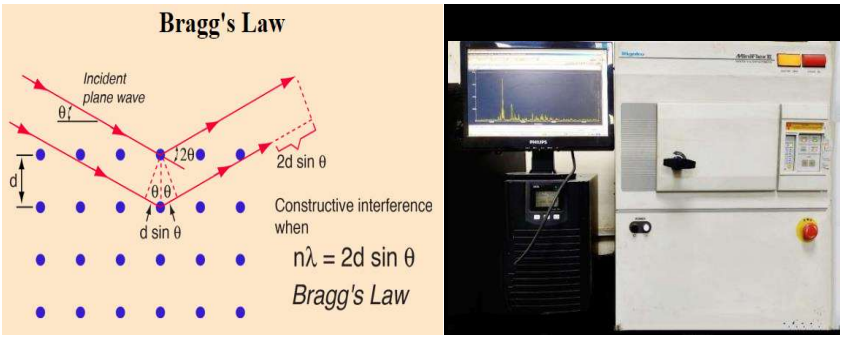

Figure 2.2: *Schematic diagram of Bragg‘s law. (b)* Image of *XRD set-up machine*.

In this technique, X-ray beams are generated by cathode rays, which are then filtered to produce monochromatic radiation. They fall on the surface of the sample after collimating to concentrate. The result of the constructive interference between the sample and the incident X-ray is a diffracted beam witch shown in Fig 2.2. At the conclusion, every diffracted ray is found, examined, and recorded. The phase identification of our samples was carried out using the Rigaku-Miniflex II DESKTOP powder X-ray diffractometer, as depicted in the figure. This diffractometer operated on a monochromatic copper source (Cu-K = 1.5418 Å) X-ray radiation at 30 kV and 15 mA.

2.2.2 X-ray Photoemission Spectroscopy (XPS) technique:

To accurately determine the chemical and physical properties of samples, it is important to accurately identify the oxidation state, elemental composition, and legend coordination. The term photoelectron spectroscopy for chemical analysis is another name for this instrument. X-ray photoelectron spectroscopy (XPS) is a technique for determining both the electronic and chemical states of components within a sample. XPS is a technique that is sensitive to the surface; therefore, it captures electrons that are created near the surface. The XPS setup is shown in Fig 2.3.

Basic Idea

The photoelectric effect, as proposed by Einstein, serves as the basis for the XPS process. Here, the compound's surface is bombarded with a monochromatic beam of photons (X-ray), and a secondary beam of electrons is expelled after the photons are absorbed by the compound. The kinetic energy (K.E.) of an electron that is ejected from the inner shell of the sample by absorption of an energy photon that falls on its surface can be determined at the XPS instrument's analyzing unit.

$$K.E. = h\upsilon - B.E. - W \quad (8)$$

Where B.E. is the binding energy of the ejected electrons and W is the work function of Spectrometer of the instrument.

The various parts of XPS spectroscopy are listed as

a) X-ray source.

b) Hemispherical electron energy analyzer

c) Vacuum system.

d) Neutralizer or electron flood gun.

e) Ar-ion gun.

f) Multi-channel detector plates.

g) Electronic control units.

h) Sample stage or holder.

i) Computer.

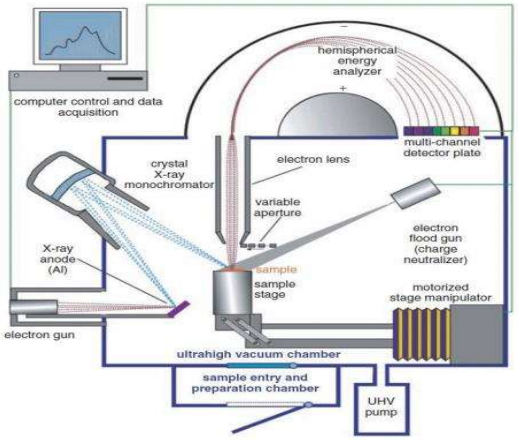

Figure 2.3: *depicts the schematic representation of the XPS setup.*

2.2.3 Raman Spectroscopy:

Utilizing Raman spectroscopy, we can determine the vibrational, rotational, and low-frequency modes of the material. In Raman spectroscopy, the radiation scattering process provides the crystal structure of the material. In previous decades, C. V. Raman discovered the optical analog of the Compton Effect in 1923, which allowed him and his research

partner Krishna to eventually discover Raman spectroscopy in 1928. This was after the discovery of Compton scattering in 1923, which occurs when electrons scatter X-rays and change their wavelength.

Basic concept

When electromagnetic radiation is dispersed on a crystal or molecule, most of the photons included are scattered elastically. Consequently, incident light and scattered photons have the same energy or wavelength. Only a small portion of light exhibits inelastic scattering. Elastic scattering is known as Rayleigh scattering, while inelastic scattering is referred to as Raman scattering. Because incident light and scattered photon frequencies differ in inelastic scattering. As a result, Raman spectra are obtained by the use of inelastic scattering of monochromatic photons. Under such circumstances, photon energy shifts might be either up or down (shifting up). Raman shift is a term provided for this change in photon energy.

Selection rule:

The change in the deformity of an atom or molecule's electron cloud is determined by molecular polarizability (α) in an electric field, the molecular deformation,

$$\text{When } \frac{d\alpha}{dQ} \neq 0 \qquad \text{[Q = normal co-ordinate]}$$

When the value of the first derivative of polarizability concerning the normal coordinate becomes non-zero, the Raman shift can be created optically. After molecular deformation, the molecules begin to vibrate at the characteristic frequency Υ_m. The light released by oscillating dipoles has frequencies of Υ_0, Υ_0-Υ_m, and $\Upsilon_0 + \Upsilon_m$ where is the frequency of light emitted by a monochromatic laser. As a result, the Raman Effect produces the three types of

scattering that are shown in the image. The scattering that corresponds to this is known as Rayleigh elastic scattering; the scattering that corresponds to the frequency $\Upsilon_0 + \Upsilon_m$ is known as anti-stokes Raman Scattering; and the scattering that corresponds to frequency $\Upsilon_0 - \Upsilon_m$ is known as Stokes Raman Scattering. Raman spectra usually display wavelengths (cm^{-1}). Thus, the Raman shift ($\Delta\omega$) can be represented by the wave number as follows:

$$\Delta\omega = \frac{1}{\lambda_0} - \frac{1}{\lambda_1} \tag{9}$$

Here are λ_1 is the wavelengths of the Raman spectrum and λ_0 the excitation. Only 5% of the power was permitted to impact the sample to avoid heating the specimen. Using a 50× long-distance objective attached to the Leica DM 2500M microscope, the laser beam was focused at a significantly shorter working distance. To maintain the same phase throughout the trials, a dispersion grating with 2400 groves/mm and a 50-micron slit width was utilized. A detector has been provided with the gathered dispersed light. The 4.0 software that was provided was used to gather the data, which was then processed once the spectrometer was scanned.

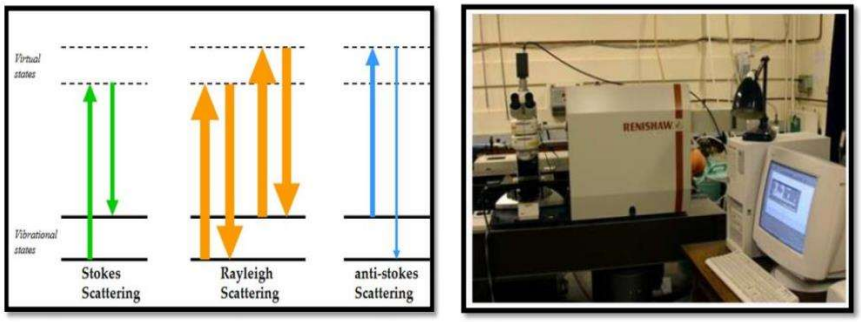

Figure 2.4: ***(a)*** *Energy level diagram of Rayleigh scattering and Raman Scattering.* ***(b)*** *Picture of Renishaw micro Raman Spectrometer.*

2.2.4 Magnetic Property Measurement System (MPMS): SQUID-VSM

We used the Quantum Design MPMS to measure the magnetization in our research. The MPMS magnetometer provides multiple measurement options for magnetization measurement in the temperature range of 1 - 400 K, utilizing a He cryostat, and in the magnetic field range of ±7.0 T. This magnetometer features an easy-to-use operating system and an extremely high sensitivity of about 10-8 emu.

Basic concept: The SQUID was initially achieved in 1963 and its operation is governed by the Josephson Effect and the flux quantization effect in superconducting rings. Two superconductors and two parallel Josephson junctions are located in this arrangement, separated by a thin insulating layer. The magnetic property was measured using three different modes in the Quantum design MPMS.

1. DC scan mode. 2. AC susceptibility mode. 3. Vibrating sample magnetometer (VSM) mode.

In our research, we utilized the vibrating sample mode. This mode is explained by Faraday's law of electromagnetic induction, which states that any circuit that changes in an electric field will also change in a magnetic field, resulting in the introduction of a magnetic field into the system. The material to be studied is put in a uniform external magnetic field while the vibrating sample mode is operating. As a result, the sample becomes magnetized because the magnetic dipole corresponds in the direction of the external field, and the net magnetic moment increases as the externally applied field increases dipole moments providing an extra field near the sample. As the material vibrates up and down over time,

this additional induced field will change. This induced current signal is monitored by a computer using a variety of software and is amplified using different electrical amplifiers. Finally, using a computer that has been calibrated using a standard sample, the signal is translated to the appropriate magnetization of the sample being studied. Using AC susceptibility mode, the spin dynamics of the material are examined. The two parameters that are obtained by measuring AC susceptibility at high frequencies are (i) θ = phase shift (ii) and the χ = AC susceptibility magnitude. Therefore, the complex variable that represents

$$\chi_{AC} = \chi' + I\,\chi''$$

AC susceptibility is χ', which stands for the in-phase or real component, and χ'' for the out-phase or imaginary component.

Figure 2.5: *Picture of Quantum Design MPMS 3 located at CIF, IIT BHU.*